

UCC Library and UCC researchers have made this item openly available. Please [let us know](#) how this has helped you. Thanks!

Title	Grasp stability and design analysis of a flexure-jointed gripper mechanism via efficient energy-based modeling
Author(s)	Kuresangsai, Pongsiri; Cole, Matthew O. T.; Hao, Guangbo
Publication date	2022-10
Original citation	Kuresangsai, P., Cole, M. O. T. and Hao, G. (2022) 'Grasp stability and design analysis of a flexure-jointed gripper mechanism via efficient energy-based modeling', IEEE Robotics and Automation Letters, 7(4), pp. 12499-12506. doi: 10.1109/LRA.2022.3220152
Type of publication	Article (peer-reviewed)
Link to publisher's version	http://dx.doi.org/10.1109/LRA.2022.3220152 Access to the full text of the published version may require a subscription.
Rights	© 2022, IEEE. Personal use of this material is permitted. Permission from IEEE must be obtained for all other uses, in any current or future media, including reprinting/republishing this material for advertising or promotional purposes, creating new collective works, for resale or redistribution to servers or lists, or reuse of any copyrighted component of this work in other works.
Item downloaded from	http://hdl.handle.net/10468/13884

Downloaded on 2022-12-08T08:31:41Z

Grasp stability and design analysis of a flexure-jointed gripper mechanism via efficient energy-based modeling*

Pongsiri Kuresangsai, Matthew O. T. Cole, and Guangbo Hao

Abstract—For flexure-based gripper mechanisms, the arrangement and design of joint elements may be chosen to allow enclosure of objects in grasping. This must provide stable containment under load, without causing excessive stress within the joint materials. This paper describes an energy-based model formulation for a cable-driven flexure-jointed gripper mechanism that can accurately describe the nonlinear load-deflection behavior for a grasped object. The approach is used to investigate the limits of grasp performance for a gripper with two single-joint fingers through simulation studies, including the accurate prediction of stability limits due to joint buckling. Hardware experiments are set up and conducted to validate the theoretical model over a range of loading conditions that exceed limits for stable grasping. Parametric design studies are also presented that show the influence of joint geometry on both grasp stability and flexure peak stress. Considering the intersection of feasible design sets, generated from simulation data over a range of possible object geometries, is shown to be an effective approach for selecting gripper design parameters.

Index Terms—Robotic gripper, compliant mechanism, grasp stability, buckling, flexure joint

I. INTRODUCTION

Compliant mechanisms are solid structures having elastic joint elements that can deform to allow motion and force transmission through the structure. The development of compliant gripper mechanisms has become a popular research field due to their suitability for grasping uncertain and delicate objects, reduced actuation/sensing requirements, and potential for simpler, lower cost construction when compared to conventional rigid-body mechanisms. Possible applications include agricultural harvesting, underwater manipulation, and

precision medical devices [1]–[6]. The use of compliance-based joints has additional benefits of reduced susceptibility to contamination and wear in comparison with bearing joints [7]. This paper deals with a special class of gripper mechanism having cable-driven flexure joints, previous examples of which include hand-like grippers [5], multi-joint fingers [8]–[10], and soft finger grippers with deformable structures [11].

A key challenge in the design of flexure-jointed grippers is that, to achieve large motion range and thereby allow enclosure of objects in grasping, highly compliant flexures are required. This can inevitably result in low stiffness of object contact, and introduces the possibility of stability-loss when grasping with high loads. A universal issue for flexure-based mechanisms is that the maximum stress should not exceed material limits for fatigue or yielding. Previously, joint topologies for a single-joint finger were analyzed by Garcia et al. [12] with the aim of minimizing flexure peak stress subject to target contact forces. Maximizing stiffness in parasitic degrees of freedom and avoiding joint buckling instabilities can also be important considerations in joint design [13], [14].

An additional concern for grasping is the ability to hold an object under the action of external disturbances, which may arise due to motion of the gripper or the application of forces to the held object [15]. In [16], the grasp stability of compliant gripper designs was assessed experimentally, where the effects from contact area, joint compliance, and finger-pad compliance were analyzed. Kragten et al. [17] developed a compliant-joint two-phalanx gripper for which the stability of the equilibrium configurations was evaluated from the eigenvalues of the Hessian matrix of the potential energy function. A thin-beam flexible gripper was evaluated based on the curvature of the potential function in [18], where the influence of object size, elastic modulus, and initial beam curvature on grasping stability were considered. Force closure properties of equilibrium configurations with friction cone constraint were applied to analyze the grasping stability and parasitic motions of a compliant adaptive hand in [19].

To formulate and solve design optimization problems for flexure-jointed mechanisms, it is important to have an efficient model of kinetostatic behavior. A mathematical description of a flexure joint element must capture its distributed nonlinear compliance properties if force-deflection behavior is to be accurately predicted. In the pseudo-rigid-body modeling (PRBM) approach, flexure elements are usually represented by one or more revolute joints [20]. More accurate representations

*Research partly supported by Chiang Mai University. Pongsiri Kuresangsai was supported by an RGJ-PhD scholarship under the National Research Council of Thailand [grant no. PHD/0101/2561]. This paper has supplementary downloadable material available at <http://ieeexplore.ieee.org>, provided by the authors. This includes a multimedia mp4 format movie clip, which gives additional information about the experimental methods. This material is 25.3 MB in size.

P. Kuresangsai was a visiting PhD student at the School of Engineering and Architecture - Electrical and Electronic Engineering, University College Cork, Ireland. He is currently with the Department of Mechanical Engineering, Chiang Mai University, Thailand. e-mail: pongsiri_kuresangsai@outlook.co.th.

M. Cole is with the Center for Mechatronic Systems and Innovation, Department of Mechanical Engineering, Chiang Mai University, Thailand, e-mail: motcole@dome.eng.cmu.ac.th.

G. Hao is with the School of Engineering and Architecture - Electrical and Electronic Engineering, University College Cork, Ireland, e-mail: G.Hao@ucc.ie.

based on multi-degree-of-freedom joints with both torsional and axial stiffness have also been proposed [9], [21]–[23]. Alternatively, a series of rigid links connected by sprung revolute joints may be considered [24], [25]. Exact analytical solutions for flexure deformation based on continuum equations can be computed from elliptical integrals in restricted cases [26], [27]. High order discretizations based on nonlinear finite element methods can also be very accurate [28], [29], but the computational complexity and lack of simple parameterizations make this approach less suitability for design analysis and optimization. This is especially true when contact interaction and motion constraints must be dealt with, as for the problem of grasp modeling that is treated in this paper. The polynomial curvature model for flexure deformation [30], which is adopted in this study, has high accuracy and efficiency and can be easily incorporated in energy-based descriptions of multi-flexure mechanism behavior [31].

This paper describes a theoretical model of a flexure-jointed gripper with two single-joint fingers and investigates how grasp load capacity can be limited by a loss of structural stability from joint buckling. The developed model is validated by experiments, for which limits of grasp stability are accurately predicted. The main contributions are listed as follows:

- 1) The definition of a reduced-order energy-based model that accurately describes the behavior of a flexure-jointed gripper mechanism by incorporating kinematic constraints for object grasping.
- 2) The identification and evaluation of key performance metrics for grasping that can be used in simulation and design studies based on the described model.
- 3) The presentation of design studies showing the feasible sets for geometric parameters in the construction of the flexure joints for avoidance of both loss of grasp stability and excessive flexure stress.

Within the paper, Section II describes the basic model for flexure behavior, Section III presents the energy-based mechanism model, incorporating grasped object kinematics, Section IV presents experimental results together with comparable model-based prediction, while Section V describes parametric design studies based on the theoretical model. The final section draws conclusions.

II. FLEXURE MODELING METHOD

This section defines the mathematical approach used to describe large deformation behavior of a thin beam flexure using a finite set of basis functions for beam curvature. This will later be incorporated within the energy-based model of a gripper mechanism during grasping, as described in Section III. The elastic deformation is assumed to follow Euler Bernoulli theory where the length of the neutral axis is fixed and all planes remain perpendicular to this axis so that the curvature is proportional to the internal bending moment.

A. Deformation model and equilibrium solution

Consider an initially straight uniform beam flexure with deformed shape described by the curvature function $\omega(\boldsymbol{\alpha}, s)$,

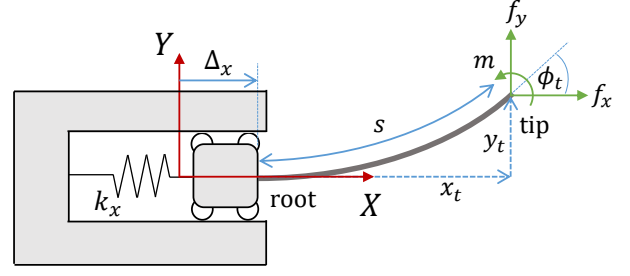


Fig. 1. Thin beam flexure model, with end loads and deformation shown.

where $s \in [0, L]$ is the distance along the neutral axis, as shown in Fig. 1. The curvature function can be approximated with a summation of basis functions $\psi_n(s)$:

$$\omega(\boldsymbol{\alpha}, s) = \frac{1}{L} \sum_{n=0}^N \alpha_n \psi_n(s) \quad (1)$$

Previous research has shown that adopting a set of smooth basis functions, such as the Legendre polynomials, can achieve accurate representation, even with low order ($N = 2$) [30]. In this formulation, the deformation variables $\boldsymbol{\alpha} = [\alpha_0, \dots, \alpha_N]^T \in \mathbb{R}^{N+1}$ need to be calculated according to the conditions for equilibrium. For the case with $N = 2$,

$$\omega(\boldsymbol{\alpha}, s) = \frac{\alpha_0}{L} + \frac{\alpha_1}{L} \left(\frac{2s}{L} - 1 \right) + \frac{\alpha_2}{L} \left(\frac{6s^2}{L^2} - \frac{6s}{L} + 1 \right) \quad (2)$$

The tangent angle is given by $\phi(\boldsymbol{\alpha}, s) = \int \omega(\boldsymbol{\alpha}, s) ds$, which is a polynomial of order $N + 1$. The location of the flexure tip relative to the initial undeflected position of the root (as indicated by the X-Y frame in Fig. 1) is given by

$$\mathbf{z}(\mathbf{p}) = \begin{bmatrix} x_t \\ y_t \\ \phi_t \end{bmatrix} = \begin{bmatrix} \Delta_x \\ 0 \\ 0 \end{bmatrix} + \int \begin{bmatrix} \cos(\phi(\boldsymbol{\alpha}, s)) \\ \sin(\phi(\boldsymbol{\alpha}, s)) \\ \delta(s-L)\phi(\boldsymbol{\alpha}, s) \end{bmatrix} ds \quad (3)$$

where $\delta(\cdot)$ is Dirac delta function and $\mathbf{p} = [\boldsymbol{\alpha}^T \Delta_x]^T$ is the vector of deformation variables. The axial deflection Δ_x of the flexure root is introduced with stiffness k_x to prevent problems of singular and non-existent solutions, which would otherwise arise due to the assumption of axial inextensibility for the flexure. In practice, k_x is chosen sufficiently large to have negligible effect on the final solution [31].

Under the aforementioned Euler-Bernoulli assumptions, the total elastic energy is given by

$$V(\mathbf{p}) = \frac{1}{2} k_x \Delta_x^2 + \frac{1}{24} E w t^3 \int_0^L (\omega(\boldsymbol{\alpha}, s))^2 ds \quad (4)$$

where E is the Young's modulus and t and w are the thickness and width of the flexure, respectively. According to (4), $V(\mathbf{p}) = \frac{1}{2} \mathbf{p}^T \mathbf{K} \mathbf{p} \geq 0$ where \mathbf{K} is given in the appendix. The method to obtain equilibrium deformation solutions is based on the Lagrangian function $\mathcal{L}(\mathbf{p}, \boldsymbol{\lambda})$ where a pre-specified tip position \mathbf{z}_0 (boundary constraint) is accounted for via the Lagrange multipliers $\boldsymbol{\lambda} = [\lambda_0 \lambda_1 \lambda_2]^T$:

$$\mathcal{L}(\mathbf{p}, \boldsymbol{\lambda}) = V(\mathbf{p}) + \boldsymbol{\lambda}^T (\mathbf{z}_0 - \mathbf{z}(\mathbf{p})) \quad (5)$$

For this energy-based formulation, equilibrium configurations must satisfy the stationary condition $\nabla_{p,\lambda}\mathcal{L} = 0$. The solution for λ then matches the external force applied at the beam tip.

B. Stress evaluation

The maximum stress due to bending can be calculated by finding the extremum points for the curvature function $\omega(s)$. These can be found as $s^* \in (0, L)$ where s^* are the solutions of $d\omega/ds = 0$. Other possible locations for maximum curvature will be the ends of the flexure ($s = 0$ and $s = L$). Hence, the maximum absolute curvature is given by

$$\bar{\omega} = \max\{|\omega(\alpha, 0)|, |\omega(\alpha, s^*)|, |\omega(\alpha, L)|\} \quad (6)$$

In general, there will be an additional contribution to stress from axial loading, which can also be taken into account. However, for a thin beam with moderate end-loads, the axial stress σ_{axial} is often negligible compared with the bending stress. Note that the peak axial stress is bounded according to $\sigma_{\text{axial}} \leq F/tw$ where $F = \sqrt{f_x^2 + f_y^2}$ with $f_x = \lambda_o$ and $f_y = \lambda_1$. Hence, the maximum stress occurring along the beam can be bounded according to

$$\sigma_{\text{max}} \leq \frac{Et}{2}\bar{\omega} + \frac{F}{tw} \quad (7)$$

where the second term can be neglected if $\bar{\omega} \gg F/Et^2w$.

III. GRASP MODELING AND STABILITY ANALYSIS

The main objective of the current study was to investigate how the limits of performance and stability in grasping relate to the properties of the flexure joint, driven by cable/tendon actuation. For this reason we focus on an idealized grasping task, but one that can also be reproduced experimentally for verification. Figure 2 shows the case where two single-joint fingers with symmetric configuration support an object subject to external load/weight W_0 acting in the x-direction. Frictionless contact with the links at points c is assumed. Each joint has a single straight beam flexure and is actuated by a cable, assumed to have zero bending stiffness.

For grasping simulation, the length of the cable can be set to produce initial contact with the object without force ($W_0 = 0$). If the cable length is fixed and the load increased, the object will move along the x-axis direction (line AB) and sliding will occur so that the contact point c moves along the link surface (assumed straight). In this situation, the displacement X_a will increase with the load W_0 and the object will be held in a stable manner if the effective grasp stiffness dW_0/dX_a is positive. It may be expected that W_0 will increase monotonically with X_a until the maximum load occurs when $dW_0/dX_a = 0$. Beyond this point the stiffness becomes negative and so the stability limit determines the maximum object load that can be supported. This fundamental limit is associated with structural buckling of the elastic flexure. It is also possible that the elastic limit of the flexure material is exceeded before the instability point is reached. These two main aspects must be considered in the analysis and design of the joint structure.

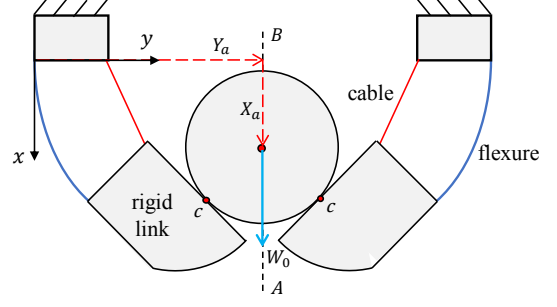


Fig. 2. Benchmark grasping task for flexure-jointed gripper.

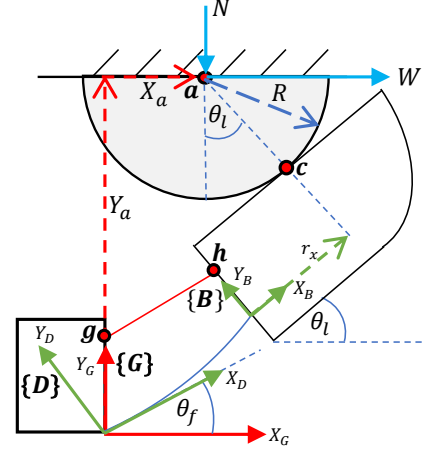


Fig. 3. Geometry for grasp modeling.

The model to predict deflection behavior of the grasped object must combine the kinematic constraints from rigid-body motion with the previously defined Lagrangian for elastic deformation of the flexure. The approach has obvious similarities with the modeling of conventional robots with compliant joints [32], [33], except that the deformation and elastic energy of a flexure joint are not captured by a single stiffness term, but rather by separate energy and kinematic constraint terms, coupled via the deformation variables p .

A. Equilibrium solution

To simulate the symmetric grasping problem, as shown in Fig. 2, it is only necessary to consider the half-space with single gripper and half object load $W = W_0/2$. This model is shown in Fig. 3, where θ_f is the flexure incline angle and θ_l is the link angle. It should be noted that $\theta_l = 0$ without joint deflection. In the global fixed frame $\{G\}$, the position of the object center is given by $P_a^G = [X_a Y_a]^T$. A loop closure constraint can be formulated in terms of the link position, which is defined by the tip position of the flexure relative to frame $\{G\}$, as given by $P_B^G = [z_x z_y]^T$, and the position r_x for the contact point c in the link frame $\{B\}$. Accordingly,

$$\mathcal{O}_c(\mathbf{q}, X_a) = P_a^G(X_a) - P_B^G - R(\theta_l)P_a^B(r_x, \theta_l) = \mathbf{0} \quad (8)$$

where $\mathbf{q} = [z_x, z_y, \theta_l, r_x]^T$ are the motion variables. The cable is constrained to pass through the fixed guiding point g

to the attachment point h on the link, and has free length L_c , so that

$$\mathcal{G}_c(\mathbf{q}) = |P_h^G(\mathbf{z}_l) - P_g^G| - L_c = 0 \quad (9)$$

Furthermore, the link position $\mathbf{z}_l = [z_x \ z_y \ \theta_l]^T$ in frame $\{G\}$ can be related to the flexure deformation variables in frame $\{D\}$ according to equation (3):

$$\mathcal{F}_c(\mathbf{q}, \mathbf{p}) = \tilde{R}(-\theta_f)\mathbf{z}_l - \mathbf{z}(\mathbf{p}) = \mathbf{0} \quad (10)$$

Note that $\mathbf{z}(\mathbf{p})$ can be evaluated numerically from (3) via a suitable discretization approach. The Lagrangian function for the flexure deformation is formulated with the constraints from equations (8) to (10):

$$\mathcal{L}(\mathbf{v}) = V(\mathbf{p}) + \lambda^T \mathcal{F}_c(\mathbf{q}, \mathbf{p}) + T \mathcal{G}_c(\mathbf{q}) + \gamma^T \mathcal{O}_c(\mathbf{q}, X_a) \quad (11)$$

Here, the multiplier T is the cable force, and $\gamma = [W \ N]^T$ combines the external forces acting on the object. All variables are combined in the vector $\mathbf{v} = [\gamma^T \ \mathbf{p}^T \ \mathbf{q}^T \ \lambda^T \ T]^T$. Equilibrium configurations (for given values of the object position X_a) are then found as solutions to $\mathbf{U}(\mathbf{v}) = \nabla_{\mathbf{v}} \mathcal{L} = \mathbf{0}$. These can be found numerically using standard multi-dimensional root finding algorithms. As the Hessian of \mathcal{L} can also be computed, gradient methods, such as those based on Newton iterations, can be applied. The main difficulty in calculating the derivatives of $\mathcal{L}(\mathbf{v})$ is due to the integral form of $\mathbf{z}(\mathbf{p})$, as given by (3), which has no closed-form representation. Formulas for computing the derivatives of $\mathbf{z}(\mathbf{p})$ based on a Gaussian quadrature discretization can be found in [30], [31]. For other terms in (11), the derivatives can be determined analytically. The use of symbolic math software (such as Maple or Mathematica) can assist greatly in achieving error-free computations.

B. Grasp stability evaluation

The grasp stiffness analysis can be performed based on the small perturbation relation for $\mathbf{U}(\mathbf{v}) = \mathbf{0}$, as given by

$$\delta \mathbf{U} = \mathbf{H} \delta \mathbf{v} + \frac{d\mathbf{U}}{dX_a} \delta X_a = \mathbf{0} \quad (12)$$

where \mathbf{H} is the Hessian matrix for \mathcal{L} : $\mathbf{H}(\mathbf{U}(\mathbf{v})) = \mathbf{J}(\nabla \mathcal{L}(\mathbf{v}))$. Hence, when \mathbf{H} is nonsingular,

$$\frac{d\mathbf{v}}{dX_a} = -\mathbf{H}^{-1} \frac{d\mathbf{U}}{dX_a} \quad (13)$$

To obtain the effective grasp stiffness K_e , we must select the appropriate element of $d\mathbf{v}/dX_a$. In our formulation, $W_0 = 2W = 2\mathbf{v}_1$, so

$$K_e = \frac{dW_0}{dX_a} = 2 \frac{d\mathbf{v}_1}{dX_a} = -2 \left\{ \mathbf{H}^{-1} \frac{d\mathbf{U}}{dX_a} \right\}_1 \quad (14)$$

Although the effective grasp stiffness K_e may be used to evaluate stability under quasi-static condition, the kinetostatic modeling approach neglects link and flexure inertia forces that impact on dynamic motion behaviors. Nonetheless, the model presented here will still be valid provided that inertia forces remain sufficiently small compared with the external force W . Under such conditions, the force-deflection behavior

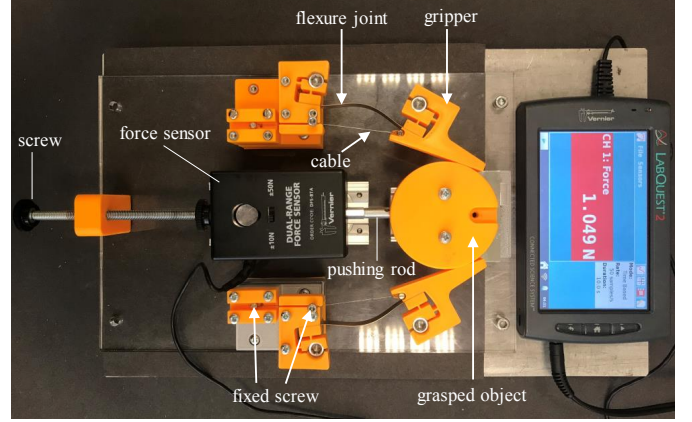


Fig. 4. Experimental setup.

of the grasped object will be little changed. This means that the external force could even be chosen to represent dynamic loading due to object acceleration. In these situations, time-based simulations would be required to determine the object motion and whether it will remain grasped, or not. The grasp-force calculation could still be based on solving the kinetostatic problem for the gripper links at each time step. Extension of the Lagrangian to include inertia forces (via kinetic energy terms) is also clearly possible, but was considered outside the scope of the present study.

IV. EXPERIMENTAL VALIDATIONS

A. Experimental setup

The experiment was devised to replicate the idealized grasping situation described in Section III. A top-down view of the system is shown in Fig. 4. The grasped object is a circular disk, which can be displaced in the horizontal plane by contact with a digital force sensor (range 0–10 N, resolution 0.01 N), moved by lead screw (with accuracy $\pm 150 \mu\text{m}$). Hence, the relation between object load W_0 and displacement X_a could be measured directly and used to determine the grasp stiffness variation. The two symmetric gripper links were connected to the fixed frame by straight flexures, attached using compliant clamps [34]. The actuation cables were attached to the gripper links with small rotating pins to reduce cable bending effects. The grasped object was also fixed to a linear guide to ensure the symmetric configuration was maintained with displacement occurring only in the X_a direction. The links and disk object were fabricated by 3-D printing in PLA material. The flexures were made from beryllium copper grade C17200 having Young's modulus $E = 125 \text{ GPa}$. Table I provides the values of the geometric parameters defined in Fig. 3. Additional joint parameters are defined in Fig. 5. The joint design parameters were chosen to allow investigation of grasping force and stability limits, while avoiding excessive strain that would lead to permanent deformation of the flexures.

B. Experimental results

For the test cases evaluated experimentally, the cable length was set to achieve a prescribed initial link angle θ_l with zero

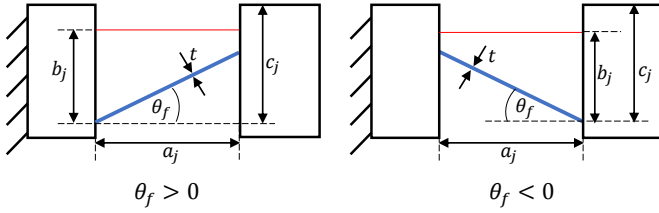


Fig. 5. Joint design parameters.

TABLE I
GEOMETRIC PARAMETERS FOR GRIPPER SYSTEM (SEE FIGS. 3 AND 5).

Description	Parameter	Value	Units
Flexure incline angle	θ_f	8.0	deg
Cable-flexure separation	b_j	10.0	mm
Gripper half-width	Y_a	60.9	mm
Object radius	R	30.0	mm
Flexure length	L	50.5	mm
Joint length (undeformed)	a_j	50.0	mm
Link depth	c_j	15.0	mm
Flexure width	w	10.0	mm
Flexure thickness	t	0.2	mm

load. Three cases were tested with initial angles of 25, 30 and 35 degrees. The object was displaced from the initial position and the load W_0 recorded over a displacement range of 0-30 mm, with data points at 2 mm intervals. Each test was repeated five times to obtain the results shown in Fig. 6. The simulation results obtained from the energy-based model described in Section III are also shown as solid lines. The two sets of results show good agreement, with maximum RMS error of 0.015 N over all cases. To obtain such high correlation, it was necessary to minimize out-of-plane effects such as twisting of the flexures and links in the experiments. This required exact symmetry and alignment of the initial configuration. The results show that the object deflection increases with load until the maximum load is reached when $dW_0/dX_a = 0$. Also, for deflections beyond this point, the grasp is unstable. The maximum load \bar{W}_0 depends significantly on the initial link angle θ_l . For these cases, where the gripper width and object radius is fixed, the maximum load increases with increasing θ_l . However, the flexure stress will also increase with θ_l . The theoretical and experimental results for maximum load \bar{W}_0 are given in Table II.

To evaluate the effective grasp stiffness K_e from the experimental results, a polynomial curve-fit was first applied to the experimental data (with order 5 achieving $R^2 \leq 0.9999$). Stiffness was then calculated from the derivative of the polynomial. Results from theory and experiment are shown in Fig. 7. A good correlation is found within the middle band of the data (5–25 mm) with maximum RMS error of 0.0011 N/mm. The trends of the experimental stiffness curves are close to the theoretical predictions, including when $K_e \approx 0$.

The results show that the energy-based modeling approach can accurately predict stability limits and load capacity for object grasping, and thus confirm its suitability for design analysis and optimization. The simulation model was also used

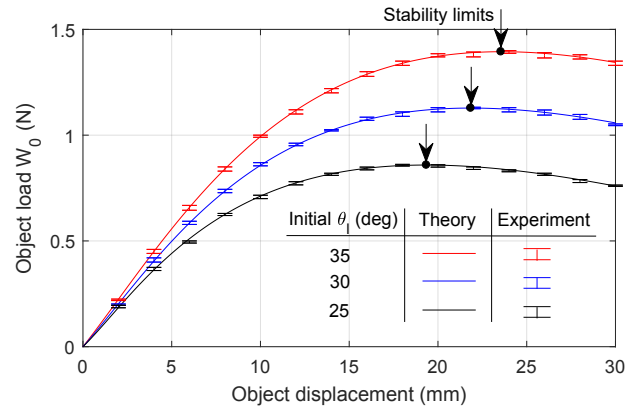


Fig. 6. Grasping load W_0 versus object displacement: Theory and experiment.

TABLE II
MAXIMUM GRASPING LOAD: THEORY AND EXPERIMENT.

Link angle θ_l (deg)	Maximum load \bar{W}_0 (N)	
	Theory	Experiment
35	1.394	1.390
30	1.128	1.123
25	0.858	0.855

to predict the peak stress that occurs in the flexures, based on the method described in Section II-B. Figure 8 shows that the peak stress increases continuously with the object displacement. The peak stress does not vary smoothly with displacement due to changes in the location of the maximum stress, from within the flexure interval $(0, L)$ to the root of the flexure $s = 0$, when the object displacement is ≈ 11 mm. The results confirm that the maximum stress for this design remains below the yield stress σ_y (965–1205 MPa).

V. DESIGN EXPLORATIONS

In this section, the metrics of effective grasp stiffness and peak stress are applied in the design of a compliant gripper. The basic geometry for the design study matches that in Fig. 3. However, the joint size is reduced compared with the experimental system, so that $a_j = 20$ mm and $b_j = 10$ mm. Also, the object radius is $R = 20$ mm and gripper half-width is $Y_a = 42.71$ mm. The design variables investigated are the flexure incline angle θ_f and flexure thickness t , which are key variables for the joint function. As the overall width of the joint b_j is fixed, two cases can be distinguished for $\theta_f > 0$ and $\theta_f < 0$, as shown in Fig. 5. In both cases, the length of the flexure is given by $L = a_j / \cos \theta_f$.

The target was to achieve a gripper design that could support a grasping load of $W_0 = 3.0$ N and allow deflection of the links up to $\theta_l = 40$ deg. As the modeling methods in Section II and III are highly efficient, it was possible to generate simulation results for a large set of design variations in short time. Data generated for design cases with $\theta_f \in (-25^\circ, 25^\circ)$ and $t \in (0.001, 0.4)$ are summarized in Figs. 9 and 10 for two different values of yield stress (1000 MPa and 690 MPa, respectively). A total of 4000 cases were generated with

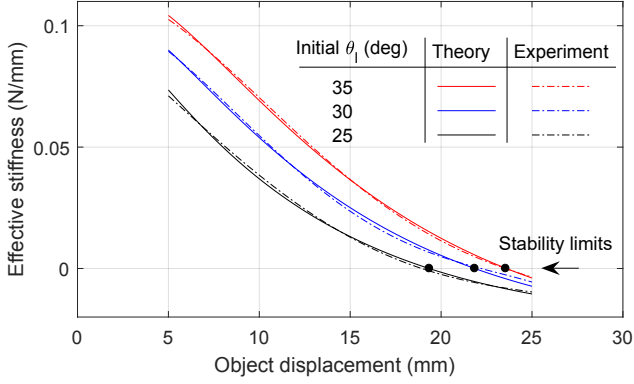


Fig. 7. Effective grasp stiffness dW_0/dX_a : Theory and experiment.

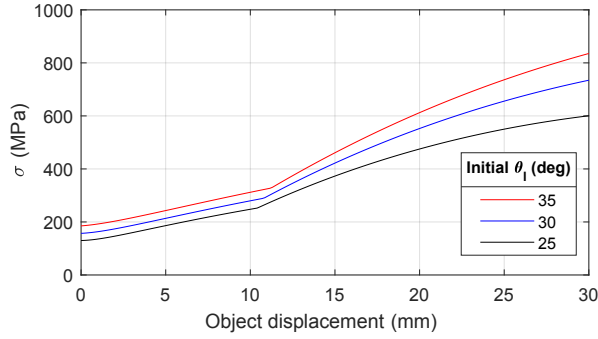


Fig. 8. Maximum stress predictions for tested cases.

uniform random distributions for θ_f and t , and simulations with increasing load up to $W_0 = 3.0$ N performed for each case. The design maps show cases that exceed the yield stress (yellow points) and cases that exceed the stability limit for $W_0 < 3.0$ N (red points). Feasible designs are indicated by blue points.

For the set of design cases with higher yield stress of 1000 MPa (Fig. 9), grasp instability tends to occur if the flexure is too thin. The flexure angle θ_f is also seen to affect grasp stability, especially for $\theta_f < 0^\circ$. The feasible design set (blue points) contains appropriate parameter values to avoid both instability and yielding. Selecting parameter values from the center of the blue region would give the most robustness to uncertainty. For the set of design cases with lower yield stress of 690 MPa, as shown in Fig. 10, the feasible set is smaller than for the previous case. However, the instability region is unchanged – the grasp stability does not depend on σ_y in the theoretical model. In these cases, yielding tends to occur if the flexure is either too thick or too thin.

Figure 11 shows the configurations obtained from simulation with two different joint designs, as detailed in Table III. These cases have similar maximum grasp loads that are limited by instability. However, the joint deformations that occur at the stability limit, as shown in Fig. 11, are very different. The limit of stability is dependent on the effective torsional stiffness of the joint, which results from the flexure beam loading condition, in combination with the geometric effects from link-

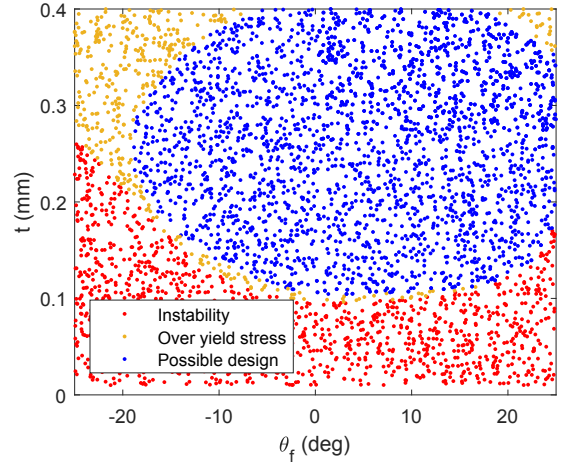


Fig. 9. Design sets for nominal grasping task with flexure yield stress $\sigma_y = 1000$ MPa.

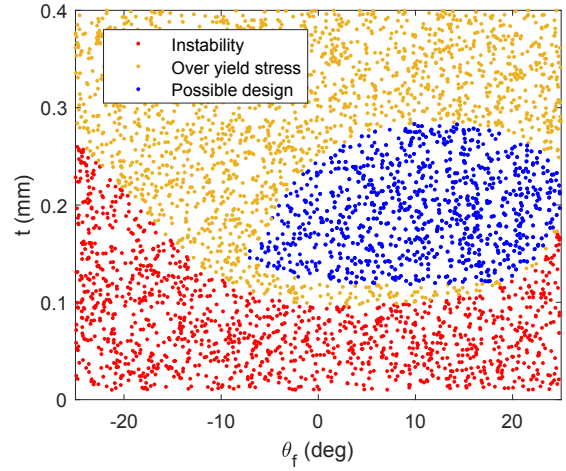


Fig. 10. Design sets for nominal grasping task with flexure yield stress $\sigma_y = 690$ MPa.

object interaction. The effective joint stiffness will tend to decrease, and the load moment from object contact increase, as θ_l decreases, leading to negative values for the effective grasp stiffness K_e . Although a basic understanding of such beam-dependent and structure-dependent loading effects can be attained from analysis [35], the effect of object geometry and motion have a complex influence, even for this simple grasping model.

Further simulations were performed to examine the effect of object size. Three sets of cases were considered with object radii $R = 15, 20$ and 25 mm. The gripper width was unchanged. The results are combined in Fig. 12, which shows the feasible design set and instability region for all three object sizes (for $\sigma_y = 690$ MPa). The results show that the feasible set is quite insensitive to the object size. Parameter values chosen from the center of this set can ensure good grasping performance for the full range of object sizes. For $\theta_f = 10^\circ$ and $t = 0.2$ mm, the maximum load is $\overline{W}_0 = 6.7$ N over all

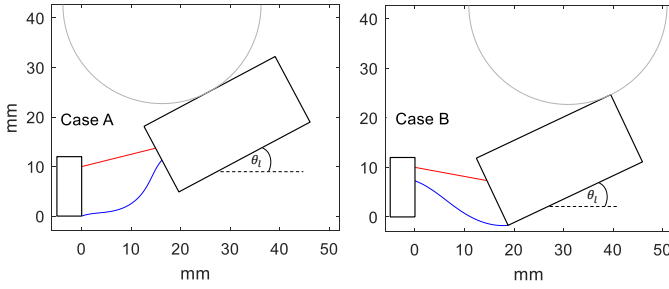


Fig. 11. Joint deformation simulation results for design cases A and B in Table III when close to stability limit.

TABLE III
DESIGN CASES WITH MAXIMUM LOAD LIMITED BY INSTABILITY.

Design case	Design parameters		Stability limit	
	θ_f (deg)	t (mm)	\bar{W}_0 (N)	θ_l (deg)
A	20	0.11	2.61	28.03
B	-20	0.21	2.72	25.28

object sizes, and is limited by yielding.

For the described design studies, flexure thickness and installation angle were chosen as design variables due to their dominant influence on gripper performance. However, other design parameters could be easily treated within the simulation-based framework, such as the initial curvature of flexures, attachment points for cables and flexures, or other link dimensions, with the possibility of improving grasp performance metrics even further.

VI. CONCLUSIONS

Predicting the behavior of a flexure-jointed gripper mechanism during object grasping is a complex problem for which the results will depend on both the gripper design and the grasped object geometry and positioning. Nonetheless, the solution of such problems is very important for design analysis and optimization. In this paper it has been shown how such predictions can be made by adopting a high efficiency model representation, and through identification and extraction of key performance metrics: namely, effective grasp stiffness and peak flexure stress.

For the considered case of a two-link cable-driven gripper, accurate predictions of load-deflection behavior and limits of stability due to joint buckling were possible. Simulation data for a large set of design cases was used to determine suitable design parameters to avoid both grasp instability and joint yielding subject to specified loading requirements. These cases showed that flexure thickness and inclination angle have an important influence on the maximum stable grasping load, and suitable values can be chosen by considering the intersection of feasible design sets generated from simulation data for a range of possible object geometries.

The described work demonstrates how it is possible to rapidly generate simulation data for a large set of design parameters and operating conditions, and use this data as a basis for selecting or optimizing mechanism and joint designs.

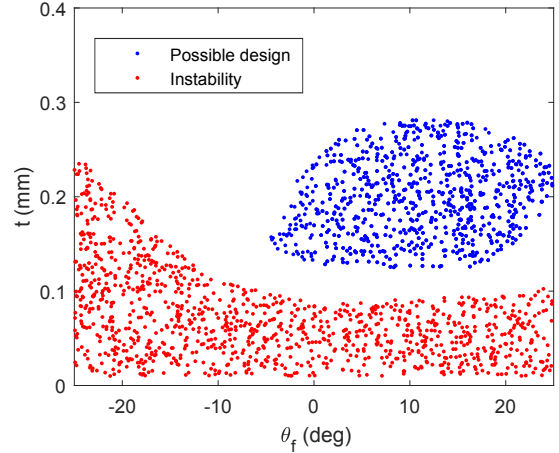


Fig. 12. Intersection of design sets for range of object radii $R = 15, 20, 25$ mm.

The described methods are suitable to be applied in the design of more complicated gripper mechanisms, such as multi-joint and multi-fingered architectures.

Currently, a main limitation of the described approach is its applicability to planar mechanisms only. Also, the treatment of dynamic effects, including link inertia, will become more important for high-speed operation. This will be considered in future work. Application in multi-objective design optimization, considering a wider range of joint architectures and geometries, is also of interest.

REFERENCES

- [1] R. R. Ma, L. U. Odhner, and A. M. Dollar, "A modular, open-source 3D printed underactuated hand," in *2013 IEEE International Conference on Robotics and Automation*, 2013, pp. 2737–2743.
- [2] K. Tai, A.-R. El-Sayed, M. Shahriari, M. Biglarbegian, and S. Mahmud, "State of the art robotic grippers and applications," *Robotics*, vol. 5, no. 2, pp. 1–20, 2016.
- [3] G. Hao and R. B. Hand, "Design and static testing of a compact distributed-compliance gripper based on flexure motion," *Arch. Civ. Mech. Eng.*, vol. 16, no. 4, pp. 708–716, 2016.
- [4] J. Shintake, V. Cacucciolo, D. Floreano, and H. Shea, "Soft robotic grippers," *Adv. Mater.*, vol. 30, no. 29, p. 1707035, 2018.
- [5] M. Liarokapis and A. M. Dollar, "Combining analytical modeling and learning to simplify dexterous manipulation with adaptive robot hands," *IEEE Trans. Autom. Sci. Eng.*, vol. 16, no. 3, pp. 1361–1372, 2019.
- [6] S. Terrile, M. Argüelles, and A. Barrientos, "Comparison of different technologies for soft robotics grippers," *Sensors*, vol. 21, no. 9, p. 3253, 2021.
- [7] K. Folkersma, S. Boer, D. Brouwer, J. Herder, and H. Soemers, "A 2-DOF large stroke flexure based positioning mechanism," in *IDETC/CIE 2012*, 2012, pp. 221–228.
- [8] G. Salvietti, I. Hussain, M. Malvezzi, and D. Prattichizzo, "Design of the passive joints of underactuated modular soft hands for fingertip trajectory tracking," *IEEE Robot. Autom. Lett.*, vol. 2, no. 4, pp. 2008–2015, 2017.
- [9] V. K. Venkiteswaran and H.-J. Su, "A three-spring pseudorigid-body model for soft joints with significant elongation effects," *J. Mech. Robot.*, vol. 8, no. 6, p. 061001, 2016.
- [10] I. Hussain, M. Malvezzi, D. Gan, Z. Iqbal, L. Seneviratne, D. Prattichizzo, and F. Renda, "Compliant gripper design, prototyping, and modeling using screw theory formulation," *Int. J. Robot. Res.*, vol. 40, no. 1, pp. 55–71, 2021.
- [11] F. Chen, W. Xu, H. Zhang, Y. Wang, J. Cao, M. Y. Wang, H. Ren, J. Zhu, and Y. F. Zhang, "Topology optimized design, fabrication, and characterization of a soft cable-driven gripper," *IEEE Robot. Autom. Lett.*, vol. 3, no. 3, pp. 2463–2470, 2018.

- [12] L. Garcia, M. Naves, and D. Brouwer, "3D-printed flexure-based finger joints for anthropomorphic hands," in *2018 IEEE/RSJ International Conference on Intelligent Robots and Systems (IROS)*, 2018, pp. 1437–1442.
- [13] G. Berselli, F. Parvari Rad, R. Vertechy, and V. Parenti Castelli, "Comparative evaluation of straight and curved beam flexures for selectively compliant mechanisms," in *2013 IEEE/ASME International Conference on Advanced Intelligent Mechatronics*, 2013, pp. 1761–1766.
- [14] S. Li and G. Hao, "Design and nonlinear spatial analysis of compliant anti-buckling universal joints," *Int. J. Mech. Sci.*, vol. 219, p. 107111, 2022.
- [15] H. Bruyninckx, S. Demey, and V. Kumar, "Generalized stability of compliant grasps," in *Proceedings. 1998 IEEE International Conference on Robotics and Automation*, 1998, pp. 2396–2402.
- [16] C.-M. Chang, L. Gerez, N. Elangovan, A. Zisimatos, and M. Liarokapis, "On alternative uses of structural compliance for the development of adaptive robot grippers and hands," *Front. Neurobot.*, vol. 13, no. 91, 2019.
- [17] G. A. Kragten, M. Baril, C. Gosselin, and J. L. Herder, "Stable precision grasps by underactuated grippers," *IEEE Trans. Robot.*, vol. 27, no. 6, pp. 1056–1066, 2011.
- [18] A. S. Vazquez, I. Payo, R. Fernandez, J. Becedas, and J. J. Jimenez, "Design parameters of flexible grippers for grasping," in *2013 IEEE International Conference on Robotics and Automation*, 2013, pp. 2060–2066.
- [19] M. V. Liarokapis and A. M. Dollar, "Post-contact, in-hand object motion compensation with adaptive hands," *IEEE Trans. Automat. Sci. Eng.*, vol. 15, no. 2, pp. 456–467, 2018.
- [20] J. Zhu and G. Hao, "Design and test of a compact compliant gripper using the Scott-Russell mechanism," *Arch. Civ. Mech. Eng.*, vol. 20, no. 3, pp. 1–12, 2020.
- [21] H. Tang and Y. Li, "Design, analysis, and test of a novel 2-DOF nanopositioning system driven by dual mode," *IEEE Trans. Robot.*, vol. 29, no. 3, pp. 650–662, 2013.
- [22] U. Bhagat, B. Shirinzadeh, L. Clark, P. Chea, Y. Qin, Y. Tian, and D. Zhang, "Design and analysis of a novel flexure-based 3-DOF mechanism," *Mech. Mach. Theory*, vol. 74, pp. 173–187, 2014.
- [23] S. Šalinić and A. Nikolić, "A new pseudo-rigid-body model approach for modeling the quasi-static response of planar flexure-hinge mechanisms," *Mech. Mach. Theory*, vol. 124, pp. 150–161, 2018.
- [24] H.-J. Su, "A pseudorigid-body 3R model for determining large deflection of cantilever beams subject to tip loads," *J. Mech. Robot.*, vol. 1, no. 2, p. 021008, 2009.
- [25] H. Mochiyama, "Model validation of discretized spatial closed elastica," in *2016 IEEE/RSJ International Conference on Intelligent Robots and Systems (IROS)*, 2016, pp. 5216–5223.
- [26] P. Wang and Q. Xu, "Design of a flexure-based constant-force XY precision positioning stage," *Mech. Mach. Theory*, vol. 108, pp. 1–13, 2017.
- [27] P. Wang, Z. Zhang, and P. Yan, "An optimized design of a large stroke beam flexure-based parallel nano manipulator," in *2015 54th IEEE Conference on Decision and Control (CDC)*, 2015, pp. 7341–7346.
- [28] M. Yang, Z. Du, and W. Dong, "Modeling and analysis of planar symmetric superelastic flexure hinges," *Precis. Eng.*, vol. 46, pp. 177–183, 2016.
- [29] G. Chen and R. Bai, "Modeling large spatial deflections of slender bisymmetric beams in compliant mechanisms using chained spatial-beam constraint model," *J. Mech. Robot.*, vol. 8, no. 4, p. 041011, 2016.
- [30] L. U. Odhner and A. M. Dollar, "The smooth curvature model: an efficient representation of Euler-Bernoulli flexures as robot joints," *IEEE Trans. Robot.*, vol. 28, no. 4, pp. 761–772, 2012.
- [31] P. Kuresangsai and M. O. T. Cole, "Kinematic modeling and design optimization of flexure-jointed planar mechanisms using polynomial bases for flexure curvature," *Mech. Mach. Theory*, vol. 132, pp. 80–97, 2019.
- [32] A. Pashkevich, A. Klimchik, and D. Chablat, "Enhanced stiffness modeling of manipulators with passive joints," *Mech. Mach. Theory*, vol. 46, no. 5, pp. 662–679, 2011.
- [33] M. Ruggiu, "On the Lagrangian and Cartesian stiffness matrices of parallel mechanisms with elastic joints," *Advanced Robotics*, vol. 26, no. 1-2, pp. 137–153, 2012.
- [34] S. Awatar and J. M. Quint, "In-plane flexure-based clamp," *Precis. Eng.*, vol. 36, no. 4, pp. 658–667, 2012.
- [35] S. Li, G. Hao, Y. Chen, J. Zhu, and G. Berselli, "Nonlinear analysis of a class of inversion-based compliant cross-spring pivots," *J. Mech. Robot.*, vol. 14, no. 3, p. 031007, 2021.

APPENDIX

The stiffness matrix for the flexure strain energy function $V(\mathbf{p}) = \frac{1}{2}\mathbf{p}^T \mathbf{K} \mathbf{p}$ follows from (1) and (4) as

$$\mathbf{K} = \begin{bmatrix} k_{00} & k_{01} & \cdots & k_{0N} & 0 \\ k_{10} & k_{11} & & k_{1N} & 0 \\ \vdots & & \ddots & & \vdots \\ k_{N0} & k_{N1} & & k_{NN} & 0 \\ 0 & 0 & \cdots & 0 & k_x \end{bmatrix}$$

where $k_{nm} = \frac{Ewt^3}{12L} \int_0^L \psi_n(s)\psi_m(s) ds$.

ACKNOWLEDGMENT

The authors gratefully acknowledge the assistance of Michael O'Shea and Timothy Power in the experimental work at UCC.